Adaptive Super-Resolution with a Synthetic Aperture Antenna

Christoph Fischer [#1], Markus Andres [*2], Hans-Ludwig Bloecher [#3], Juergen Dickmann [#4], Wolfgang Menzel [*5]

[#] *Daimler AG, Environment Perception*
Wilhelm-Runge-Strasse 11, 89081 Ulm, Germany
[1] christoph.c.fischer@daimler.com
[3] hans-ludwig.bloecher@daimler.com
[4] juergen.dickmann@daimler.com

[*] *University of Ulm, Institute of Microwave Techniques*
Albert-Einstein-Allee 41, 89069 Ulm, Germany
[2] markus.andres@uni-ulm.de
[5] wolfgang.menzel@uni-ulm.de

***Abstract*—This work proposes an efficient way to implement super-resolution in a radar sensor based on digital beamforming and presents first measurements and a performance comparison. For full exploitation of the available aperture size, the sensor utilizes multiple transmitters to form a synthetic aperture almost twice the size of the physical aperture. Super-resolution techniques are applied to the larger aperture. These algorithms have a high computational complexity. To minimize this effort, a target selection based on CFAR algorithms is performed before the actual super-resolution step. Measurement results show the performance of the proposed algorithm in real life scenarios.**

***Index Terms*—Super-resolution, Linear Prediction, OS-CFAR, Millimeter-Wave Radar, Automotive Radar**

I. Introduction

Modern environment perception has an increasing demand for accuracy of target positions and separability of multiple targets. Radar sensors have the advantage of being weather independent and play an important role in today's automotive sensor instrumentation. Compared to cameras or Lidar sensors, they have the disadvantage of low angular resolution. This can be improved by increasing the aperture of the antenna, but design and construction aspects limit this freedom significantly. Application of synthetic aperture techniques can increase the angular resolution of a given sensor notably whilst only slightly increasing the physical size of the antenna system [1]. In combination with super-resolution techniques, e.g., the well known MUSIC Algorithm [2], this can lead to a much better exploitation of a given aperture size than in current sensor configurations. When using super-resolution techniques, computational complexity is a major factor that has to be taken into account. In this work, a technique for selective super-resolution using CFAR techniques (e.g. OS-CFAR, cf. [3]) is applied. Computational complexity can be reduced considerably by this means because cells containing only noise or clutter are neglected before processing.

This paper is structured as follows. First, an outline of the applied beamforming method in combination with the synthetic aperture is given. In the next section, the used super-resolution algorithm is described and subsequently, the combination of both with the selective processing approach is explained. Finally, the developed method is applied to real world measurements, and a short performance comparison and a conclusion are given.

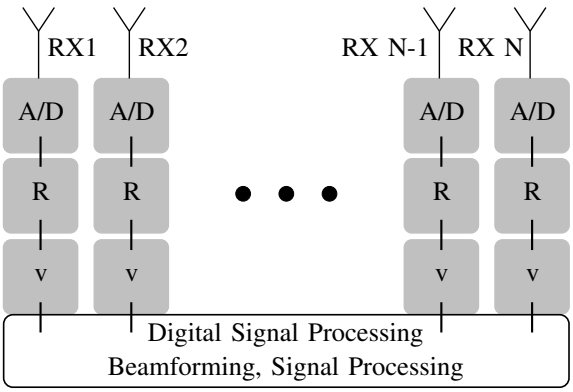

Fig. 1. Block diagram of the receive side of a digital beamforming radar sensor using N parallel receive channels.

II. Digital Beamforming with a Synthetic Aperture Receive Array

The simplest form of a digital beamforming (DBF) system consists of a single transmit antenna illuminating the desired field of view (FoV) completely, in combination with a number of receive antennas. In FMCW radar sensors, the receive signals of these elements are down-converted and then sampled and quantized in parallel to form the signals $s_m[i]$ (with the sampling index m of the time signal and the receiver index i, the sampling index is omitted in the following because only spatially sampled signals are considered). The beamforming takes place in the successive digital signal processor (see Figure 1). In a sensor using the FMCW modulation, this beamforming step can be conducted for every single ramp. In a system using two separate transmit antennas as introduced in [1], these antennas transmit independent signals (commonly using time multiplex). After receiving these two signals, the

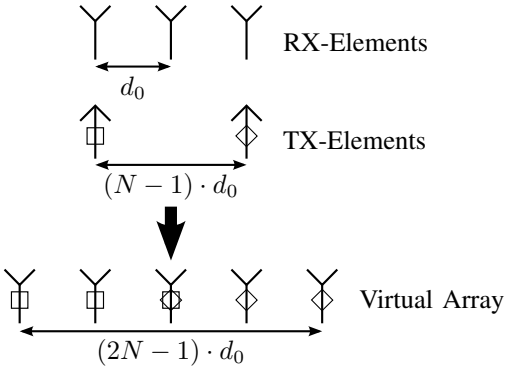

Fig. 2. Illustration of the DBF principle with synthetic aperture using three receive and two transmit elements [1].

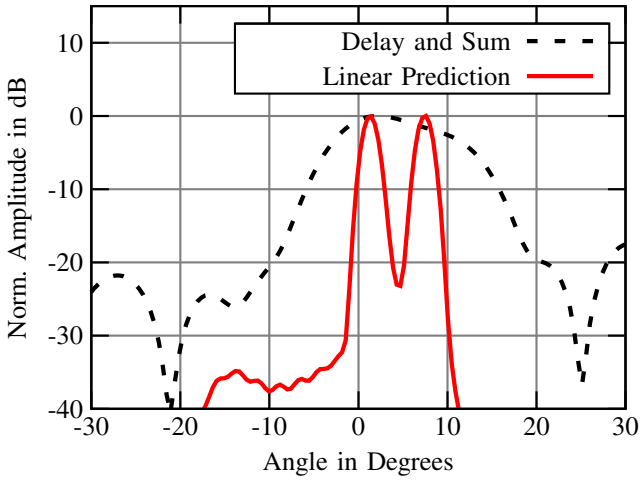

Fig. 3. Amplitude plot of a measured signal from two closely spaced corner reflectors using beamforming with delay and sum, and linear prediction.

beamforming is performed identically to a standard array with the virtual dimensions as depicted in Figure 2. Notably, the aperture of the virtual array is nearly twice the physical aperture of the DBF antenna array. The position $r_{\text{virt}}(x)$ of the virtual receive antennas can be described mathematically by the convolution of the positions of the physical receive antennas $r_{\text{RX}}(x)$ and the transmit antennas $r_{\text{TX}}(x)$

$$r_{\text{virt}}(x) = r_{\text{RX}}(x) \otimes r_{\text{TX}}(x). \tag{1}$$

An example is shown in Figure 2. It can be seen that the center element of the resulting virtual array consists of two real elements with the same virtual position. This fact can be used for calibration purposes because the elements with the same position should also receive identical signals. If the signal-to-noise-and-clutter ratio is sufficiently high, possible deviations between the two receive channels (resulting from differences in the two transmitters or from Doppler shifts of moving targets) can be compensated by this means.

For a uniform linear array (ULA) with a constant distance d_0 between the elements, the classical beamforming itself is performed by evaluating

$$f(\varphi, k) = \sum_{i=0}^{N-1} s_k[i] \cdot \exp\left(\mathrm{j}2\pi \frac{i d_0}{\lambda} \sin\varphi\right) \tag{2}$$

for any desired viewing angle φ. This method is known as delay and sum, or Bartlett beamformer. The phases of the incident signals are adjusted for constructive interference in a certain beam direction. The amplitudes can be tapered in addition to the phase adjustment to minimize side lobes. In other fields, this tapering is also known as windowing.

In the following chapter more sophisticated techniques for direction finding are presented. These techniques have the advantage of higher performance that comes with higher computational demands.

III. Super-Resolution Techniques

In classical beamforming using the delay and sum algorithm, the beamwidth and therefore the ability to separate two targets angularly is determined by the aperture of the antenna. Using the synthetic aperture technique from [1], it is possible to almost double the available aperture. In automotive applications, the limit for the smallest possible 3dB-beamwidth considering space restrictions is on the order of 2° for a 77 GHz sensor. With algorithms like MUSIC or linear-prediction based approaches, it is possible to achieve better results (cf. [4] or [5]) with regard to angular separation with a given aperture size. An example is shown in Figure 3. With delay and sum beamforming, the two corner reflectors cannot be resolved but with linear prediction two distinct maxima are visible. A linear-prediction based super-resolution algorithm has been selected because such an approach allows replacing the delay and sum beamforming block by the one using linear prediction while leaving all subsequent steps unchanged. Another advantage is the structure of the prediction itself. It can be realized as a digital filter with tunable coefficients which can be implemented efficiently using available hardware (i.e., DSPs or FPGAs). With these advantages and similar performance to MUSIC or other DOA algorithms, linear prediction has been selected for further use and will be described shortly in the following.

The idea of the algorithm is to build an appropriate filter that, when excited with the original signal (in our case the spatially sampled antenna outputs), generates an extrapolated version thereof [6]. By this means the antenna aperture appears to be larger and therefore the 3dB-beamwidth of the expanded array becomes smaller than that of the physical antenna. Several steps are necessary to compute the extrapolated signal. First, the coefficients c_l of the digital filter need to be found. This filter has order P, the number of expected spatial frequencies in the signal. Burg's Algorithm [7] minimizes the expectance of the quadratic prediction error of the signal $s[i]$ and its prediction $s_e[i]$. After finding the filter coefficients c_l, the prediction is performed in forward and backward direction using

$$s_e[i] = \begin{cases} \sum_{l=1}^{P} c_l s[i-l] & \forall\, i \geq 0, \\ \sum_{l=1}^{P} c_{P-l+1}^{*} s[i+P-l+1] & \forall\, i < 0. \end{cases} \tag{3}$$

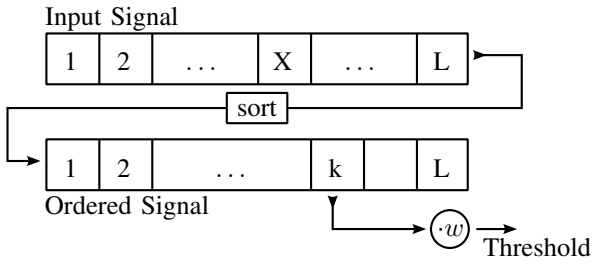

Fig. 4. Block diagram of the used OS-CFAR algorithm. X is the cell under test and k is the index of the selected noise sample in the ordered signal.

Once the expanded signal $s_e[i]$ is obtained, the beamforming can be conducted analog to the delay and sum approach whilst considering the larger virtual aperture. Another advantage of the linear prediction approach is that it is not as sensitive to the selection of the model order P as, for example, with MUSIC. For different measurements, it has been found to make sense to set the model order to a fixed value (e.g. 5) and do all processing with that value. The order can be chosen relatively low because targets are not only separated by angle but also in Doppler and range domain.

IV. Adaptive super-resolution

A key issue for the proposed algorithm is reliable detection of signals after range processing. The range-Doppler processing step is done prior to all other steps and can be computed in parallel for all individual receive channels (cf. Figure 1). Next, a peak detection is conducted individually for each channel using a CFAR algorithm. The results presented here have been obtained using an ordered statistic (OS) CFAR for which a simple block diagram is shown in Figure 4. A continuous block of L samples is selected from the signal. The signal values inside this window are then sorted, and the k-over-L quantile of the set is taken as an estimation for the noise level contained inside this window. This noise value is then weighted to give the threshold for declaring signal detection. An example for different sets of parameters that result for different thresholds is shown in Figure 5. In this figure, the noise floor is about 30 dB below the maximum amplitude of the narrow band signal at slightly above 200 Hz. The signal is clearly above all three thresholds and will therefore be declared as a detection in either case. The green, circled curve shows an unwanted increase around the peak that may hide targets with low amplitude in multi target environments with high dynamic range (e.g. a pedestrian standing beside a car).

A very important factor for CFAR algorithms is the false alarm probability P_{fa}. For OS-CFAR, P_{fa} is given in [8] by

$$P_{fa} = \prod_{j=1}^{k-1} \frac{L-j}{L-j+w}. \tag{4}$$

For final target detection in radar systems, a very low false alarm probability is desired (in the order of $P_{fa} \ll 10^{-3}$). In the case considered here, there should be no degradation of detection performance, especially for distributed targets

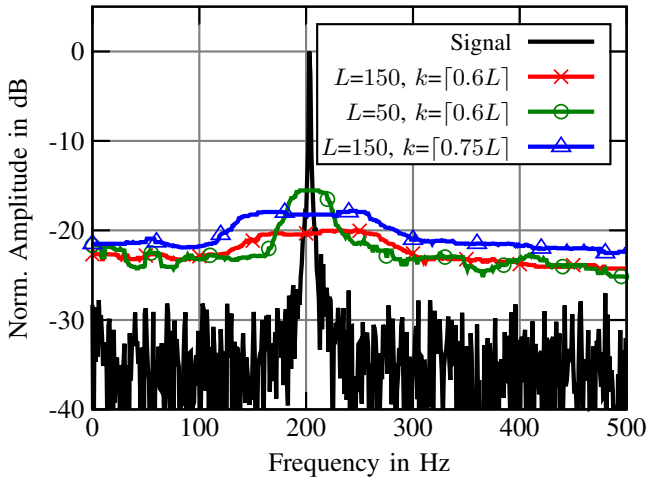

Fig. 5. Amplitude plot for a simulated signal with noise and the computed thresholds for different sets of CFAR parameters (w=3.5 for all thresholds).

where super-resolution can resolve important features of the object that would have gone unrecognized with delay and sum beamforming. For this reason the choice of parameters is L=29, k=$\lceil 0.6 \cdot L \rceil$ and w=4.0. With these parameters, the false alarm probability is P_{fa}=0.038 and has proven to be sufficiently sensitive even for the detection of weak targets.

After the detection in a single channel, the signals are combined in the beamforming block. Whenever a detection is made in a single channel, the super-resolution beamforming is performed according to the previous section and the results are subsequently fed to another CFAR stage operating in the same manner with respect to the angular direction. Subsequently, the detected peaks are passed to the following processing stage, most likely the clustering and target generating stage that are both beyond the scope of this work. In the next section, some measurement results and comparisons are presented.

V. Measurements and results

The overall time to compute a single radar image has been evaluated based on one exemplary scenario. The time needed to acquire the data (i.e. read the file with the measurement data from the hard disk) is not included. The radar sensor used for the presented measurement utilizes the 76–77 GHz automotive radar band and uses the chirp sequence waveform for range-Doppler signal separation according to [9]. Range resolution is 0.5 m and 10 physical antennas are used for beamforming.

The scene used for the measurements is shown in Figure 6. It has been selected because it shows many targets in different range cells, and at the same time, has objects in the same range cell on opposite sides of the street. It represents a realistic scenario for an inner city street with a road sign on the left (marked A), lamp posts on the right (marked B and C), benches and possible road clutter from curbs.

Figure 7 depicts the scene with straightforward application of the linear prediction algorithm. The individual targets are visible as well as some clutter resulting from side lobes

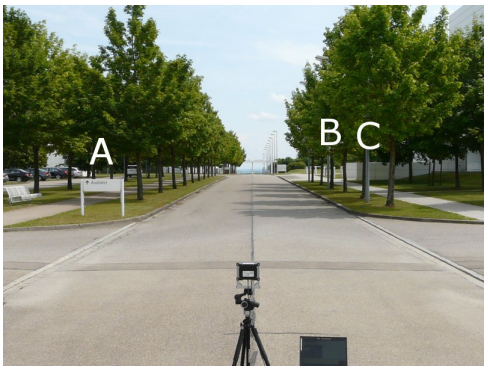

Fig. 6. Image of the scene used for the radar image. Strong targets have been marked (A: road sign; B, C: lamp post).

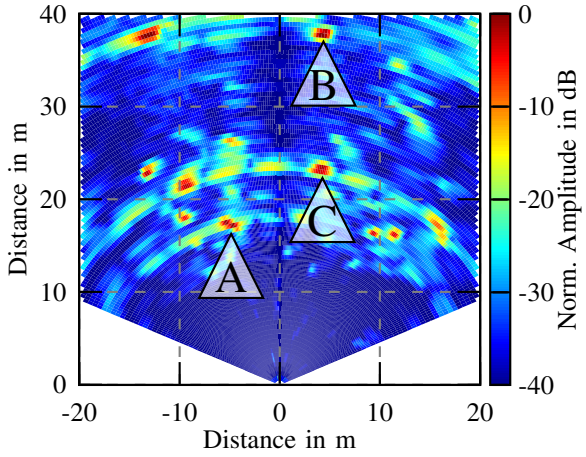

Fig. 7. Intensity plot of the measured scene obtained using linear prediction without target selection and with three targets marked according to Figure 6.

TABLE I
TABLE SHOWING THE PROCESSING TIME FOR CFAR, NON CFAR AND CLASSICAL DELAY AND SUM.

Parameter	Lin. Pred.	Lin. Pred. + CFAR	Del. and Sum
Processing Time	T_{proc}	$0.11 \cdot T_{\text{proc}}$	$0.018 \cdot T_{\text{proc}}$

of the antenna pattern. The result using the target selection approach prior to the linear prediction is displayed in Figure 8 (with application of a subsequent CFAR processing in angular direction). Here, the individual targets are still visible but a great part of the scene is empty, representing areas with no reflectors. The computational effort for the two radar images is indicated in Table I (where Lin. Pred. relates to Figure 7 and Lin. Pred. + CFAR relates to Figure 8), along with the relative processing time for delay and sum beamforming (i.e. processing of the scene without super-resolution) for comparison. The time for the target selection approach also includes the subsequent peak detection in angle after the beamforming. It can be seen that using target preselection, computation time goes down by almost one order of magnitude.

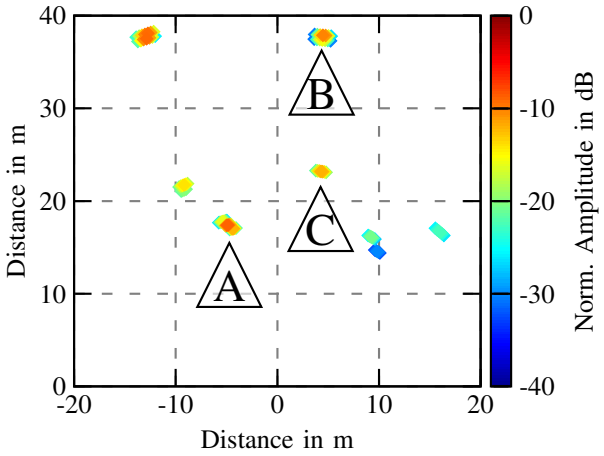

Fig. 8. Intensity plot of the measured scene obtained using linear prediction with target selection and with three targets marked according to Figure 6.

VI. CONCLUSION

Super-resolution algorithms like MUSIC or linear prediction have the potential to exploit the performance of a given digital beamforming sensor beyond the bounds of standard approaches like delay and sum beamforming at the cost of computational complexity. This work presented a simple method for reducing this cost to a manageable amount by solely processing range cells that are likely to contain a target while dropping empty cells. By this means, the processing time needed for computing a frame of a super-resolution digital beamforming system could be improved by one order of magnitude. Further research may lead to even better results using different CFAR methods or super-resolution techniques. The proposed algorithm should also be implemented in hardware using a fast signal processor to verify whether its application is as effective in practice as in the calculations.

REFERENCES

[1] N. Kees, E. Schmidhammer, and J. Detlefsen, "Improvement of angular resolution of a millimeterwave imagingsystem by transmitter location multiplexing," in *Microwave Systems Conference, 1995. Conference Proceedings., IEEE NTC '95*. IEEE, May 1995, pp. 105–108.

[2] R. Schmidt, "Multiple emitter location and signal parameter estimation," *IEEE Transactions on Antennas and Propagation*, vol. 34, no. 3, pp. 276–280, Mar. 1986.

[3] H. Rohling, "Radar CFAR Thresholding in Clutter and Multiple Target Situations," *IEEE Transactions on Aerospace and Electronic Systems*, vol. AES-19, no. 4, pp. 608–621, 1983.

[4] M. Schoor and B. Yang, "High-Resolution Angle Estimation for an Automotive FMCW Radar Sensor," in *International Radar Symposium, IRS*, Sep. 2007.

[5] P. Feil, W. Mayer, and W. Menzel, "Various cross-range resolution techniques applied to an eight-channel 77GHz sensor," in *European Radar Conference*, Oct. 2007, pp. 59–62.

[6] J. Makhoul, "Linear prediction: A tutorial review," *Proceedings of the IEEE*, vol. 63, no. 4, pp. 561–580, Apr. 1975.

[7] J. P. Burg, "Maximum Entropy Spectral Analysis," Ph.D. dissertation, Dept. of Geophysics, Stanford University, Stanford, CA, May 1975.

[8] P. P. Gandhi and S. A. Kassam, "Analysis of CFAR processors in homogeneous background," *Aerospace and Electronic Systems, IEEE Transactions on*, vol. 24, no. 4, pp. 427–445, Jul. 1988.

[9] A. G. Stove, "Linear FMCW radar techniques," *Radar and Signal Processing, IEE Proceedings F*, vol. 139, no. 5, pp. 343–350, Oct. 1992.